Group theory analysis of phonons in two-dimensional transition metal dichalcogenides

J. Ribeiro-Soares,[1,2,*] R. M. Almeida,[1] E. B. Barros,[2,3] P. T. Araujo,[4] M. S. Dresselhaus,[2,5] L. G. Cançado,[1] and A. Jorio[1]

[1]*Departamento de Física, Universidade Federal de Minas Gerais, Belo Horizonte, Minas Gerais, 30123-970, Brazil*

[2]*Department of Electrical Engineering and Computer Science, Massachusetts Institute of Technology (MIT), Cambridge, Massachusetts 02139, USA*

[3]*Departamento de Física, Universidade Federal do Ceará, Fortaleza, Ceará, 60455-900, Brazil*

[4]*Department of Physics and Astronomy, University of Alabama, Tuscaloosa, Alabama 35487, USA*

[5]*Department of Physics, Massachusetts Institute of Technology (MIT), Cambridge, Massachusetts 02139, USA*

Transition metal dichalcogenides (TMDCs) have emerged as a new two-dimensional material's field since the monolayer and few-layer limits show different properties when compared to each other and to their respective bulk materials. For example, in some cases when the bulk material is exfoliated down to a monolayer, an indirect-to-direct band gap in the visible range is observed. The number of layers N (N even or odd) drives changes in space-group symmetry that are reflected in the optical properties. The understanding of the space-group symmetry as a function of the number of layers is therefore important for the correct interpretation of the experimental data. Here we present a thorough group theory study of the symmetry aspects relevant to optical and spectroscopic analysis, for the most common polytypes of TMDCs, i.e., $2Ha$, $2Hc$ and $1T$, as a function of the number of layers. Real space symmetries, the group of the wave vectors, the relevance of inversion symmetry, irreducible representations of the vibrational modes, optical activity, and Raman tensors are discussed.

PACS number(s): 62.25.Jk, 63.22.Np, 68.35.Gy, 78.20.Ek

I. INTRODUCTION

The interest in two-dimensional (2D) layered materials increased after the successful isolation of monolayer graphene (the 2D component of graphite) reported in 2004 [1]. The monolayer of hexagonally-linked carbon atoms made it possible to study a brand-new set of magnetic, electric, and optical phenomena related to the Dirac-like nature of graphene electrons [2]. The lack of a band gap, however, imposes some difficulties to graphene's application in electronics, despite its high carrier mobility.

Other classes of 2D materials are now also being intensively studied for many different applications motivated mainly by the need of a band gap. Perovskite-based oxides, van der Waals solids such as Bi_2Se_3, Bi_2Te_3 [3], hexagonal boron nitride (h-BN) [4], and transition metal dichalcogenides (TMDCs), such as MoS_2 and WSe_2 [5–7], offer a wide range of compounds and combinations with potential use in the emerging field of 2D heterostructures [8] (for example, tunable optoelectronic properties are obtained by a suitable choice of component layers [9,10]). The TMDCs are layered materials of the form MX_2, where M stands for groups 4–10 of transition metals and X stands for the chalcogen atoms S, Se, or Te [11]. The M and X atoms are strongly linked through covalent bonds to form 2D layers. Two adjacent sheets of chalcogen atoms are separated by a sheet of transition metal atoms in an X-M-X configuration, and the "monolayer" is actually composed of an atomic trilayer (TL) structure. The interaction among these trilayers are weak van der Waals interactions. The difference in the stacking order gives rise to different polytypes, while the combination of these different atoms leads to a variety of

more than 30 different layered materials, with different optical, mechanical and electrical properties [11–13].

Some semiconducting TMDCs in this so-called monolayer form show a direct band gap in the visible range, which does not exist in their bulk counterparts [5–7,14,15]. These band gaps open the possibility for flexible and transparent sensor applications [11,12,16], and the construction of heterostructures offers the possibility of tuning the TMDC behavior [9,10,16]. The breaking of inversion symmetry in the monolayer, with the strong spin-orbit interaction coming from the metal d orbitals, gives rise to the spin splitting of the valence band at the high-symmetry K points of the Brillouin zone (BZ) [17]. Since the K and K' points in the BZ are related to each other by time reversal symmetry, the spin splitting yields distinct symmetries from these two valleys, and the manipulation of this coupling opens the possibility of a variety of valleytronic applications [17–22].

The dependence on the number of layers (N) and on the changes of the symmetry group have already been investigated in the characterization of the various TMDC optical properties, by means of Raman spectroscopy and second harmonic generation (SHG) [21,23–29]. Group theory provides a valuable theoretical tool that can be used to understand the selection rules for the optical transitions, to find the eigenvectors for the lattice vibrations, and to identify the lifting of degeneracies due to external symmetry-breaking perturbations [30,31]. A detailed study of these symmetry aspects for few-layers TMDCs is valuable to predict interesting characteristics and to properly interpret experimental results for these compounds, since few-layers TMDCs will belong to different space groups according to the number of layers, and their space groups will be different from those of their bulk crystal counterparts.

Group theory has already been used to describe the structure of TMDCs in the bulk form for different polytypes [32,33], in the few-TL $2Hc$ polytype for zone center phonons (at the Γ BZ point) [23–25] and for the electronic structure at the

*Author to whom correspondence should be addressed: jenainas-soares2@gmail.com

Γ and K points [34], and for a more detailed understanding of some nonlinear optical processes [26]. In this work, group theory is applied to TMDCs in both the trigonal prismatic (H) and octahedral (T) metal atom coordinations, considering the stacking order for $2Ha$ and $2Hc$ for H, and $1T$ for T, and the dependence on the number of layers N (even or odd), and considering the full set of wave vectors in the BZ, i.e., going beyond the zone center. In Sec. II, the symmetry analysis in real space is developed for the $2H$ (Sec. II A 1) and $1T$ (Sec. II A 2) polytypes, while the reciprocal space treatment is shown in Sec. II B. The relevance of inversion symmetry for the different TMDCs polytypes is discussed in Sec. II C. The irreducible representations for vibrational modes for few-TL TMDCs considering the high-symmetry points and lines in the BZ are presented in Sec. II D, and the Raman and infrared selection rules are shown in Sec. II E, while Sec. II F gives the Raman tensors. Finally, Sec. III summarizes the main conclusions and comments on the cases of lowering of symmetry induced by strain in MoS_2, by engineering heterostructures, and by breaking the out-of-plane translational symmetry in WSe_2.

II. SYMMETRY ANALYSIS

A. Real space symmetry

The family of layered TMDCs is composed of several polytypes with a different number of TLs, or different metal atom coordinations that form the primitive unit cell (see Table I). The main polytypes under experimental and theoretical consideration nowadays (and analyzed in the present work) are the trigonal prismatic $2H$ [two TLs in a trigonal prismatic coordination (H) are required to form the bulk primitive unit cell] and the octahedral $1T$ [one TL in an octahedral coordination (T) is required to form the bulk primitive unit cell] (see Fig. 1). Each polytype, in turn, has a monolayer (one TL) as a basic 2D building block unit. The bulk crystal is made by piling up these monolayer units, namely $1H$ (trigonal prismatic or AbA coordination, where upper cases represent chalcogen atoms and lower cases represent metal atoms) and $1T$ (octahedral or AbC coordination), as can be observed in Figs. 1(a) and 1(b), respectively. The blue spheres represent transition metal atoms, and the orange spheres represent the chalcogen atoms. For bulk versions of these layered materials, where the out-of-plane translational symmetry is present, the lateral views of the unit cells are highlighted with red rectangles in Figs. 1(c), 1(d), and 1(e).

There are several other polytypes for stacks of more than two TLs, and at least 11 polytypes were identified in TMDCs [33]. For example, the unit cell of the $3R$-MoS_2 (with the stacking /AbA BcB CaC/)[32,33] comprises nine atoms in three TLs. The treatment of these polytypes with a high number of TLs is beyond the scope of this work, but for the $3R$ case, Table I summarizes some symmetry considerations and gives representative TMDC examples.

1. 2H *polytype*

The $2H$ bulk polytype can assume two forms with different stacking symmetries: $2Ha$ (or /AbA CbC/ stacking) [32,33], and $2Hc$ (/CaC AcA/ stacking) [33]. In $2Ha$ stacking, one transition metal atom is always on top of another transition

TABLE I. Number of structural formulas (Z), space groups and Wyckoff positions for $2H$, $1T$, and $3R$ TMDCs polytypes. One structural formula comprises one transition metal (M) and two chalcogen atoms (X_2).

Polytype	$2Ha$ polytype			$2Hb$ polytype[a]		$2Hc$ polytype			$3R$ polytype[a]		$1T$ polytype		
Number of layers	Bulk	N odd	N even	Bulk		Bulk	N odd	N even	Bulk		Bulk	N odd and N even	
# Structural formulas (Z)	2	N	N	2		2	N	N	3		1	N	
Group[b]	D_{6h}^4 ($P6_3/mmc$, #194)	D_{3h}^1 ($P\bar{6}m2$, #187)	D_{3d}^3 ($P\bar{3}m1$, #164)	D_{3h}^1 ($P\bar{6}m2$, #187)		D_{6h}^4 ($P6_3/mmc$, #194)	D_{3h}^1 ($P\bar{6}m2$, #187)	D_{3d}^3 ($P\bar{3}m1$, #164)	C_{3v}^5 ($R3m$, #160)		D_{3d}^3 ($P\bar{3}m1$, #164)	D_{3d}^3 ($P\bar{3}m1$, #164)	
Wyckoff positions[b,c]	M (2b) X (4f)			M_1 (1a) M_2 (1d) X_1 (2h) X_2 (2i)		M (2c) X (4f)			M (3a) X_1 (3a) X_2 (3a)		M (1a) X (2d)		
Compounds[a]	(Nb,Ta)(S,Se,Te)$_2$			Nb$_{1+x}$Se$_2$ Ta$_{1+x}$Se$_2$		Mo(S,Se,Te)$_2$ W(S,Se)$_2$			(Nb,Ta)(S,Se)$_2$ (Mo,W)S$_2$		(Ti,Zr,Hf,V)(S,Se,Te)$_2$ (Nb,Ta)(S,Se)$_2$		

[a]According to previous literature on TMDCs [32,33].
[b]The fact that 3D space groups and the respective Wyckoff positions have been constructed considering translation along the out-of-plane direction does not change the conclusions that will be drawn in the present work because we disregard the wave vector along this nonexisting direction.
[c]The Wyckoff positions for the space groups of N odd and N even layers of TMDCs are not established in the International Tables of Crystallography [35].
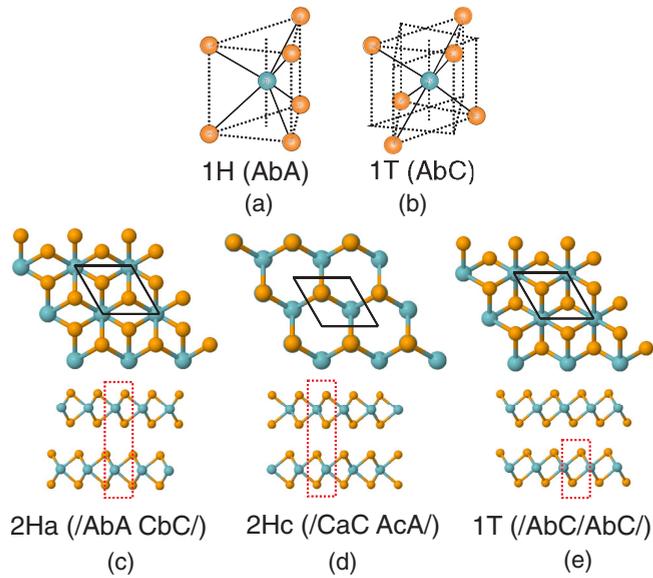
FIG. 1. (Color online) Transition metal atom coordination for (a) trigonal prismatic (H) and (b) octahedral (T) TMDCs polytypes. The blue spheres represent transition metal atoms and orange ones, chalcogen atoms. In (c), (d), and (e) the top and lateral views (top and bottom in each figure, respectively) of the primitive unit cells for bulk TMDCs materials are shown. The black rhombuses show the top view of the primitive unit cell, and the red rectangles indicate the lateral view. The primitive unit cell of the (c) $2Ha$ or the (d) $2Hc$ polytypes comprise six atoms, two transition metal atoms, and four chalcogenides ($Z = 2$) in the trigonal prismatic coordination illustrated in (a), while the $1T$ polytype shown in (e) has three atoms, comprising two chalcogenides, and one transition metal atom ($Z = 1$) in the octahedral coordination illustrated in (b).
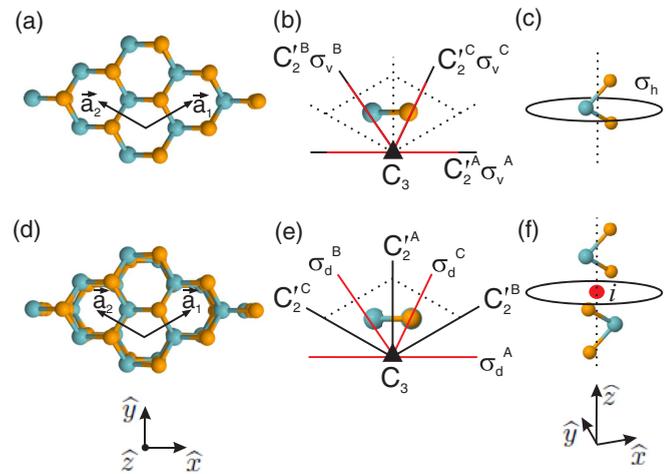

FIG. 2. (Color online) Primitive unit cell and symmetry operations of the $2Hc$ polytype. Blue spheres represent transition metal atoms and orange spheres represent chalcogen atoms. (a) and (d) show the top view for the 1TL and 2TLs, respectively. $\vec{a}_1$ and $\vec{a}_2$ are the primitive unit vectors, indicated in (a), while (b) and (e) represent the symmetry operations for the 1TL and 2TLs, respectively. The C_3 axes are perpendicular to the xy plane in (b) and (e), and they are represented by black triangles. Three vertical mirror planes σ_v and three dihedral mirror planes σ_d are indicated as red lines in (b) and (e), respectively, while the black lines are the three C_2' rotation axes in the horizontal mirror σ_h, represented in (c) and (f) together with the primitive unit cell. The σ_h itself is not a symmetry operation for 2TLs, but it is discussed here since it is part of the S_6 operation, which is given as a C_6 rotation followed by a σ_h reflection in this plane. The red lines in (e) denote the σ_d mirror planes, and the red dot in the center of (f) indicates the position of the inversion symmetry operation.

metal atom of the next layer, as shown in Fig. 1(c). This polytype is reported to occur in NbSe$_2$, NbS$_2$, TaS$_2$, and TaSe$_2$ crystals [32]. In $2Hc$ stacking, any transition metal atom is sitting on top of two chalcogenides atoms of the subsequent layer, as shown in Fig. 1(d). This polytype occurs in MoS$_2$, WS$_2$, MoSe$_2$, and WSe$_2$ crystals. Both polytypes belong to the nonsymmorphic hexagonal space group $P6_3/mmc$ [32] (D_{6h}^4 in Schönflies notation, or #194 in the International Tables for Crystallography Vol. A (ITCA) [35]). The primitive unit cell for the bulk has six atoms ($Z = 2$, where Z is the number of structural MX_2 units required to form the primitive unit cell), and three atoms in each TL, as can be seen in the red rectangles of Figs. 1(c) and 1(d). The Wyckoff positions for the $2H$ bulk polytypes, as well as the number of structural formulas Z are given in Table I.

The $2Hb$ polytype is possible and occurs for nonstoichiometric compounds with an excess of metal atoms intercalated in the van der Waals gap [33]. Table I gives symmetry information and examples for this polytype. Some differences between the definition of $2Hb$ and $2Hc$ are found in the literature [32,33], and the most recent nomenclature is used in this work [33,36].

For few-layer systems there is a reduction in symmetry due to the lack of translational symmetry along the z axis (the z axis is perpendicular to the basal plane of the TLs). The symmetry operations are reduced from 24 in the bulk to 12 for both even and odd numbers of TLs. Therefore, the few-TLs space groups are different from the bulk space groups and depend on the parity of the number of layers (even or odd number of TLs). Figure 2 illustrates the 1TL and 2TL stacking arrangements for the $2Hc$ polytype. The hexagonal real space for 1TL and 2TLs are given in Figs. 2(a) and 2(d), respectively.

The $2Hc$ polytype symmetry operations are illustrated in Figs. 2(b) and 2(e), which are the top-views of the primitive unit cells. In Figs. 2(c) and 2(f), the lateral views of the primitive unit cells are given for 1TL and 2TLs, respectively. The space groups of few-layer TMDCs can be renamed according to the "layered subperiodic groups", from the International Tables for Crystallography Vol. E (ITCE) [37], but here we adopt the ITCA nomenclature [35] for comparison with related literature [38]. The 1TL of the $2H$ polytype belongs to the $P\bar{6}m2$ (D_{3h}^1 or #187) hexagonal symmorphic space group, as well as to other few-layer compounds with odd number of layers, whose point symmetry operations are E (identity), $2C_3$ [clockwise and anticlockwise rotations of $120°$ about the axis represented as a black triangle in Fig. 2 (b)], $3C_2'$ (two-fold axis in the σ_h plane), σ_h (the horizontal reflection plane that passes through the transition metal atom), $2S_3$ (C_3 clockwise and anticlockwise rotations, followed by a σ_h reflection), and $3\sigma_v$ (vertical reflection planes).

The 2TLs of $2H$ polytype and any other even number of TLs belong to the D_{3d}^3 ($P\bar{3}m1$, #164) symmorphic space group, whose symmetry operations are E, $2C_3$, $3C_2'$ [rotation axes placed in between two adjacent TLs, i.e., in the middle of the van der Waals gap in Fig. 2(f)], inversion i [red dot in the σ_h plane of Fig. 2 (f)], $3\sigma_d$ [dihedral vertical mirror planes represented by red lines in Fig. 2 (e)], and $2S_6$ (clockwise and anticlockwise rotations of $60°$ followed by a σ_h reflection). For the 3TLs case, when another TL unit is added to the 2TLs shown in Figs. 2(d), 2(e), and 2(f), the symmetry operations are the same as those observed for 1TL, since the σ_h plane is recovered as a symmetry operation. The addition of subsequent layers will always show symmetry variations depending on whether the number of layers is odd or even, and the difference between these two groups is ultimately given by the presence of the inversion symmetry in 2TLs (which is absent in 1TL) and the presence of the σ_h plane in 1TL (which is absent in 2TLs).

2. 1T polytype

From a symmetry standpoint, the $1T$ polytype is constructed by piling up single 1TL units, where each subsequent layer is exactly the same as the previous one, with one transition metal atom (or chalcogen atom) on top of another transition metal atom (or chalcogen atom), in an octahedral coordination. In the bulk TMDC, the stacking is /AbC/AbC/ (see Fig. 1). The bulk form belongs to the D_{3d}^3 ($P\bar{3}m1$, #164) symmorphic space group. The unit cell comprises three atoms of one TL [red rectangle in Fig. 1(e)]. The Wyckoff positions and number of structural formulas (Z) for the $1T$ polytype TMDCs are given in Table I. Because all layers are identical, the symmetry operations do not change by increasing the number of TLs, no matter if N is even or odd. Figures 3(a) and 3(d) show the 1TL and 2TLs structures, respectively, of the $1T$ polytype. The symmetry operations of 1TL are E, $2C_3$, $3C_2'$ [the C_2' rotation axes are in the reflection plane, between the two chalcogen atoms, dividing in half the transition metal atom, as shown in the black lines in Fig. 3 (c)], inversion i (red dot in the transition metal atom), $3\sigma_d$ [dihedral vertical mirror planes represented by red lines in Fig. 3(b)], and $2S_6$ (clockwise and anticlockwise rotations of $60°$ followed by a σ_h reflection). In the 2TL case, the same operations are still valid, but now the inversion and the reflection plane [Fig. 3(f)] for the S_6 operation are located in the van der Waals gap.

B. Group of the wave vector

The reciprocal space high-symmetry points and directions for the $2H$ and $1T$ polytypes are shown in Fig. 4. Here $\vec{a}_1$ and $\vec{a}_2$ are the primitive vectors of the real 2D lattice described by Eq. (1) and are shown in Fig. 2(a). Correspondingly, $\vec{b}_1$ and $\vec{b}_2$ [described in Eq. (2)] are the reciprocal lattice vectors shown in Fig. 4.

$$\vec{a}_1 = \frac{a}{2}(\sqrt{3}\hat{x} + \hat{y}), \quad \vec{a}_2 = \frac{a}{2}(-\sqrt{3}\hat{x} + \hat{y}), \quad (1)$$

$$\vec{b}_1 = \frac{2\pi}{a}\left(\frac{\sqrt{3}}{3}\hat{k}_x + \hat{k}_y\right), \quad \vec{b}_2 = \frac{2\pi}{a}\left(-\frac{\sqrt{3}}{3}\hat{k}_x + \hat{k}_y\right). \quad (2)$$
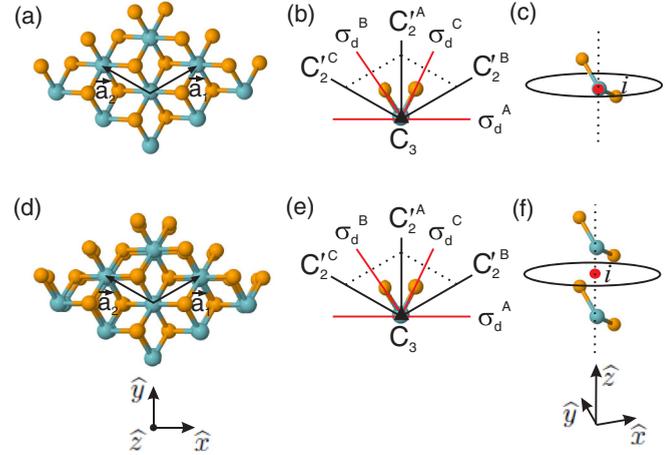

FIG. 3. (Color online) Primitive unit cells and symmetry operations of the $1T$ TMDCs polytypes (bulk, 1TL and 2TLs). (a) and (d) show the 1TL and 2TL top view. In (d), chalcogen atoms are on top of chalcogen atoms, and transition metal atoms are on top of transition metal atoms, giving a similar top view to that observed for 1TL. In (b) and (e), the C_3 rotation axes (represented as black triangles) are perpendicular to the basal plane. The red lines represent σ_d mirror planes, while the black lines stand for C_2' rotation axes that lie in the σ_h plane. The primitive unit cells for 1TL (and bulk) and for 2TLs are shown in (c) and (f), respectively, and the red dot in their centers denotes the inversion operations. Notice that σ_h is not a symmetry operation for 1TL (or N odd), 2TLs (or N even), or bulk, but the reflection plane is shown here to indicate the reflection in the two S_6 operations.

The differences between the space groups D_{3h}^1 and D_{3d}^3 when the number of TLs is odd or even define different symmetries for the group of the wave vectors (GWV) at each high-symmetry point or direction of the reciprocal space. Knowledge of the GWV is important because the invariance of the Hamiltonian under symmetry operations usually leads to degeneracies at these high-symmetry points or directions in the BZ [39–41]. The GWV for the $2H$ TMDCs is similar
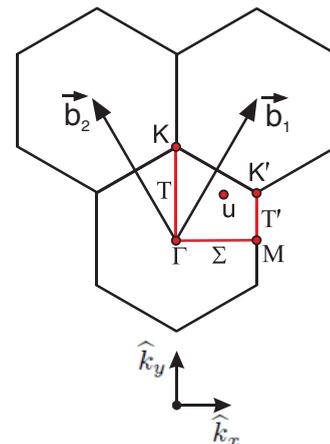

FIG. 4. (Color online) The Brillouin Zone (BZ) symmetries: Γ, K, K', and M are high-symmetry points; the T, T', and Σ are high-symmetry lines, and the u denotes the symmetry for a generic point. $\vec{b}_1$ and $\vec{b}_2$ denote the in-plane reciprocal lattice vectors.

to the GWV found for N-layer graphene and bulk graphite [38], since the space groups for bulk, N even, and N odd ($N \geqslant 3$) TLs in the TMDC family resemble the corresponding graphene systems. However, the 1TL case in TMDCs lacks inversion symmetry and therefore belongs to the same space group ($P\bar{6}m2$) as that for other N-odd layers. Table II shows the groups that are isomorphic to the GWV for all the BZ high-symmetry points and axes occurring for bulk and for both odd or even number of TLs in the $2H$ polytype.

The $1T$ polytype has the same GWV regardless the number of layers in the sample. The bulk is symmorphic, so it has the same GWV. Table III shows the GWV for different high-symmetry points and axes within the BZ for this polytype.

C. Relevance of inversion symmetry

The presence or absence of inversion symmetry is an important aspect of TMDCs since it opens the possibility of coupled spin and valley physics [17]. The strong spin-orbit coupling in TMDC materials is due to the d orbitals in their heavy metal atoms. The absence of inversion symmetry lifts the degeneracy of the same energy at the same $\bar{k}$ value, at the K point of the BZ, and spin splitting values on the order of 0.4 eV have been observed in WSe$_2$ [21].

The inversion symmetry is also important for optics, e.g., the second-harmonic generation (SHG) technique, which has been routinely used to probe not only the presence of inversion symmetry, but also the crystal orientation [26,27] and, recently, the effect on SHG of two artificially stacked TMDCs layers [42]. For centrosymmetric crystals, the $\chi^{(2)}$ nonlinear susceptibility vanishes [43], and no SHG signal is observed. The $2H$ TMDCs polytype (and in this case, also including the 1TL) belong to the noncentrosymmetric space group D_{3h}^1 and then it is possible to observe a SHG signal [21,26–28,42–44]. The N-even TLs for $2H$ TMDCs do not show SHG since their space groups are centrosymmetric. For the $1T$ TMDCs polytype, both N-even and N-odd TLs have the same centrosymmetric space group D_{3d}^3, and the SHG signal is not expected. In this sense, the SHG mapping (together with other characterization tools) could be used to detect different polytypes in the same sample since the $2H$ polytype with an odd number of layers shows SHG, while the layered $1T$ polytype does not.

D. Irreducible representations for vibrational modes

The irreducible representations for the lattice vibrations (Γ^{vib}) are given by the direct product $\Gamma^{vib} = \Gamma^{eq} \oplus \Gamma^{vec}$, where Γ^{eq} denotes the equivalence representation for the atomic sites, and Γ^{vec} is the representation for the x, y and z real space vectors [40]. The Γ^{vec} representation can be written as $\Gamma^{vec} = \Gamma^x \oplus \Gamma^y \oplus \Gamma^z$, or $\Gamma^{vec} = \Gamma^{x,y} \oplus \Gamma^z$ when x and y have the same irreducible representation. The Γ^{vib} representations for the $2Ha$, $2Hc$, and $1T$ polytypes are given in Tables IV, V, and VI, respectively, for all the BZ high-symmetry points and lines (shown in Fig. 4), and for odd or even numbers of TLs. It is worth noting that for the $2Hc$ polytype, the Γ^{vib} for the K' point is the complex conjugated form of the Γ^{vib} for the K point, while for the $2Ha$ polytype the atomic sites are different (due to different Wyckoff positions) and the Γ^{vib} of the K and K' points are the

TABLE II. Space groups and group of the wave vector (GWV) according to the number N of TLs for all high-symmetry points and lines in the BZ of the $2H$ polytype of TMDCs.

	Space group	Γ	$K(K')$	M	$T(T')$	Σ	u
N odd	D_{3h}^1 ($P\bar{6}m2$, #187)	D_{3h}^1 ($P\bar{6}m2$, #187)	C_{3h}^1 ($P\bar{6}$, #174)	C_{2v}^{14} ($Amm2$, #38)	C_s^{xy} (or C_s^1, Pm, #6)[a]	C_{2v}^{14} ($Amm2$, #38)	C_s^{xy} (or C_s^1, Pm, #6)
N even	D_{3d}^3 ($P\bar{3}m1$, #164)	D_{3d}^3 ($P\bar{3}m1$, #164)	D_3^2 ($P321$, #150)	C_{2h}^3 ($C2/m$, #12)	C_2^3 ($C2$, #5)	C_s^{xz} (or C_s^3, Cm, #8)[b]	C_1^1 ($P1$, #1)
Bulk	D_{6h}^4 ($P6_3/mmc$, #194)	D_{6h}^4 ($P6_3/mmc$, #194)	D_{3h}^4 ($P\bar{6}2c$, #190)	D_{2h}^{17} ($Cmcm$, #63)	C_{2v}^{16} ($Ama2$, #40)	C_{2v}^{14} ($Amm2$, #38)	C_s^{xy} (or C_s^1, Pm, #6)[a]

[a]"xy" denotes the σ's mirror plane.
[b]"xz" denotes the σ's mirror plane.

TABLE III. Space group and group of the wave vector (GWV) for the high-symmetry points and directions in the BZ for $1T$ polytype in TMDCs, valid for N-layer (even or odd) and bulk.

Space group	Γ	$K(K')$	M	$T(T')$	Σ	u
D_{3d}^3 ($P\bar{3}m1$, #164)	D_{3d}^3 ($P\bar{3}m1$, #164)	D_3^2 ($P321$, #150)	C_{2h}^3 ($C2/m$, #12)	C_2^3 ($C2$, #5)	C_s^{xz} (or C_s^3, Cm, #8)[a]	C_1^1 ($P1$, #1)

[a]"xz" denotes the σ's mirror plane.

same. In the $1T$ polytype, the Γ^{vib} for the K and K' points is also the same. The conversion from the space group (SG) to the point group (PG) notation for the irreducible representations is indicated in each character table of the Supplemental Material [45]. The irreducible representations for vibrations for each high-symmetry point and line of the BZ for the bulk polytypes are also given in Tables SI, SII, and SIII of the Supplemental Material [45].

E. Raman and infrared activity

For bulk $2H$ polytypes ($1T$ polytype), the lattice vibration irreducible representations Γ^{vib} for the 18 (9) zone center phonons are reproduced in the first line of Table VII (see also Tables SI and SII from the Supplemental Material) [45]. The classification of the modes as Raman active, infrared (IR) active, acoustic, and silent are given in Table VII.

For the 2D polytypes, the Raman and IR active modes show symmetry variations depending on the number of layers since the high-symmetry Γ points have different GWV. The GWV at the Γ point is D_{3h}^1 for N-odd $2H$ polytypes, D_{3d}^3 for N-even $2H$ polytypes, and D_{3d}^3 for the N-even and N-odd $1T$ polytype. The total number of modes for N even or N odd layers in the $2H$ and $1T$ polytypes, including their classification as Raman active, IR active, acoustic, and silent modes are given in Tables VIII and IX, respectively.

In the $1T$ polytype, since the space group is the same in both N-even and N-odd, the representations for the few-TL films of this polytype refer to the same irreducible representations of the group of the wave vector D_{3d}^3 at the Γ point, which in turn are the same as those found for its bulk counterpart.

F. Raman tensors

To define whether or not a specific vibrational mode will be experimentally observed in a given Raman scattering geometry, we use here the Porto notation [46,47], which indicates the crystal orientation with respect to the polarization and propagation directions of the laser. Four letters are used

in the Porto notation to describe the scattering process in the a(bc)d form: while "a" and "d" are the propagation directions of the incident and scattered light, respectively, "b" and "c" represent the polarization directions for the incident and scattered light, respectively. One common Raman experimental geometry is the backscattering configuration, where the incident and scattered light have an opposite sense. For example, in the $\bar{z}(xy)z$ configuration the $\bar{z}$ and z are the directions of the incident and scattered light, with the opposite sense, x is the polarization direction of the incident light, and y is the polarization direction of the scattered light.

The Raman scattering intensity given by the Hamiltonian perturbation term is proportional to $|\widehat{e}_s \cdot \overleftrightarrow{\alpha} \, \widehat{e}_i|^2$, where $\widehat{e}_s$ is the unit vector along the polarization direction of the scattered light, $\widehat{e}_i$ is the unit vector along the polarization direction of the incident light, and $\overleftrightarrow{\alpha}$ is the Raman tensor. The quadratic functions ($xx, xy, xz, yz, ...,$) indicate the irreducible representations for the Raman-active modes. Following this procedure, the Raman tensors for all the Raman active modes of N-layer thin films can be found. For the $2H$ polytype with N-odd few layers (D_{3h}^1 group of the wave vector for the Γ point), the Raman tensors are [48]

$$\Gamma_1^+(A_1') : \begin{pmatrix} a & 0 & 0 \\ 0 & a & 0 \\ 0 & 0 & b \end{pmatrix},$$

$$\Gamma_3^+(E')_{(x)} : \begin{pmatrix} 0 & d & 0 \\ d & 0 & 0 \\ 0 & 0 & 0 \end{pmatrix}, \quad \Gamma_3^+(E')_{(y)} : \begin{pmatrix} d & 0 & 0 \\ 0 & -d & 0 \\ 0 & 0 & 0 \end{pmatrix},$$

$$\Gamma_3^-(E'') : \begin{pmatrix} 0 & 0 & 0 \\ 0 & 0 & c \\ 0 & c & 0 \end{pmatrix}, \begin{pmatrix} 0 & 0 & -c \\ 0 & 0 & 0 \\ -c & 0 & 0 \end{pmatrix}.$$

For the N-even $2H$ polytype, and for the N even or odd for the $1T$ polytype, as well as for the $1T$ bulk crystal (D_{3d}^3

TABLE IV. Normal vibrational mode irreducible representations (Γ^{vib}) for the N-layer TMDCs $2Ha$-polytype (/AbA CbC/), considering all the high-symmetry points and lines in the BZ.

	$2Ha$-polytype (/AbA CbC/)	
	N odd	*N* even
Γ	$\left(\frac{3N-1}{2}\right)(\Gamma_1^+ \oplus \Gamma_3^-) \oplus \left(\frac{3N+1}{2}\right)(\Gamma_3^+ \oplus \Gamma_2^-)$	$\left(\frac{3N}{2}\right)(\Gamma_1^+ \oplus \Gamma_3^+ \oplus \Gamma_2^- \oplus \Gamma_3^-)$
$K(K')$	$\left(\frac{3N-1}{2}\right)(K_1^+ \oplus K_2^- \oplus K_2^{-*}) \oplus \left(\frac{3N+1}{2}\right)(K_2^+ \oplus K_2^{+*} \oplus K_1^-)$	$\left(\frac{3N}{2}\right)(K_1 \oplus K_2) \oplus 3NK_3$
M	$3N(M_1 \oplus M_4) \oplus \left(\frac{3N-1}{2}\right)M_2 \oplus \left(\frac{3N+1}{2}\right)M_3$	$3N(M_1^+ \oplus M_2^-) \oplus \left(\frac{3N}{2}\right)(M_2^+ \oplus M_1^-)$
Σ	$3N(\Sigma_1 \oplus \Sigma_4) \oplus \left(\frac{3N-1}{2}\right)\Sigma_2 \oplus \left(\frac{3N+1}{2}\right)\Sigma_3$	$6N\Sigma_1 \oplus 3N\Sigma_2$
$T(T')$	$\left(\frac{9N+1}{2}\right)T^+ \oplus \left(\frac{9N-1}{2}\right)T^-$	$\left(\frac{9N}{2}\right)(T_1 \oplus T_2)$
u	$\left(\frac{9N+1}{2}\right)u^+ \oplus \left(\frac{9N-1}{2}\right)u^-$	$9Nu$

TABLE V. Normal vibrational mode irreducible representations (Γ^{vib}) for the N-layer TMDCs $2Hc$-polytype (/CaC AcA/), considering all the high-symmetry points and lines in the BZ.

	$2Hc$-polytype (/CaC AcA/)	
	N odd	N even
Γ	$\left(\frac{3N-1}{2}\right)(\Gamma_1^+ \oplus \Gamma_3^-) \oplus \left(\frac{3N+1}{2}\right)(\Gamma_3^+ \oplus \Gamma_2^-)$	$\left(\frac{3N}{2}\right)(\Gamma_1^+ \oplus \Gamma_3^+ \oplus \Gamma_2^- \oplus \Gamma_3^-)$
$K(K'^*)$	$\left(\frac{3N+1}{2}\right)(K_1^+ \oplus K_2^+ \oplus K_2^{-*}) \oplus \left(\frac{3N-1}{2}\right)(K_1^- \oplus K_2^- \oplus K_2^{+*})$	$\left(\frac{3N}{2}\right)(K_1 \oplus K_2) \oplus 3NK_3$
M	$3N(M_1 \oplus M_4) \oplus \left(\frac{3N-1}{2}\right)M_2 \oplus \left(\frac{3N+1}{2}\right)M_3$	$3N(M_1^+ \oplus M_2^-) \oplus \left(\frac{3N}{2}\right)(M_2^+ \oplus M_1^-)$
Σ	$3N(\Sigma_1 \oplus \Sigma_4) \oplus \left(\frac{3N-1}{2}\right)\Sigma_2 \oplus \left(\frac{3N+1}{2}\right)\Sigma_3$	$6N\Sigma_1 \oplus 3N\Sigma_2$
$T(T')$	$\left(\frac{9N+1}{2}\right)T^+ \oplus \left(\frac{9N-1}{2}\right)T^-$	$\left(\frac{9N}{2}\right)(T_1 \oplus T_2)$
u	$\left(\frac{9N+1}{2}\right)u^+ \oplus \left(\frac{9N-1}{2}\right)u^-$	$9Nu$

TABLE VI. Normal vibrational mode irreducible representations (Γ^{vib}) for the N-layer TMDCs $1T$-polytype (/AbC/AbC/), considering all the high-symmetry points and lines in the BZ.

	$1T$-polytype (/AbC/AbC/)	
	N odd	N even
Γ	$\left(\frac{3N-1}{2}\right)(\Gamma_1^+ \oplus \Gamma_3^+) \oplus \left(\frac{3N+1}{2}\right)(\Gamma_2^- \oplus \Gamma_3^-)$	$\left(\frac{3N}{2}\right)(\Gamma_1^+ \oplus \Gamma_3^+ \oplus \Gamma_2^- \oplus \Gamma_3^-)$
$K(K')$	$\left(\frac{3N-1}{2}\right)K_1 \oplus \left(\frac{3N+1}{2}\right)K_2 \oplus 3NK_3$	$\left(\frac{3N}{2}\right)(K_1 \oplus K_2) \oplus 3NK_3$
M	$(3N-1)(M_1^+ \oplus M_1^-) \oplus \left(\frac{3N-1}{2}\right)M_2^+ \oplus (3N+1)M_2^-$	$3N(M_1^+ \oplus M_2^-) \oplus \left(\frac{3N}{2}\right)(M_2^+ \oplus M_1^-)$
Σ	$6N\Sigma_1 \oplus 3N\Sigma_2$	$6N\Sigma_1 \oplus 3N\Sigma_2$
$T(T')$	$\left(\frac{9N-1}{2}\right)T_1 \oplus \left(\frac{9N+1}{2}\right)T_2$	$\left(\frac{9N}{2}\right)(T_1 \oplus T_2)$
u	$9Nu$	$9Nu$

TABLE VII. Normal vibrational mode irreducible representations (Γ^{vib}) for bulk TMDCs at the Γ point within the $2Ha$, $2Hc$, and $1T$ polytypes. The Raman active, infrared active, acoustic, and silent mode irreducible representations are identified.

	$2Ha$ and $2Hc$ polytypes	$1T$ polytype
Γ^{vib}	$\Gamma_1^+ \oplus 2\Gamma_3^+ \oplus \Gamma_5^+ \oplus 2\Gamma_6^+ \oplus 2\Gamma_2^- \oplus \Gamma_4^- \oplus 2\Gamma_5^- \oplus \Gamma_6^-$	$\Gamma_1^+ \oplus \Gamma_3^+ \oplus 2\Gamma_2^- \oplus 2\Gamma_3^-$
Raman	$\Gamma_1^+ \oplus \Gamma_5^+ \oplus 2\Gamma_6^+$	$\Gamma_1^+ \oplus \Gamma_3^+$
Infrared	$\Gamma_2^- \oplus \Gamma_5^-$	$\Gamma_2^- \oplus \Gamma_3^-$
Acoustic	$\Gamma_2^- \oplus \Gamma_5^-$	$\Gamma_2^- \oplus \Gamma_3^-$
Silent	$2\Gamma_3^+ \oplus \Gamma_4^- \oplus 1\Gamma_6^-$	-

TABLE VIII. Normal vibrational mode irreducible representations (Γ^{vib}) for the N-layer TMDCs at the Γ point within the $2Ha$ and $2Hc$ polytypes. Raman active, infrared active, acoustic, and silent mode irreducible representations are identified.

	$2Ha$ and $2Hc$ polytypes	
	N odd	N even
Γ^{vib}	$\left(\frac{3N-1}{2}\right)(\Gamma_1^+ \oplus \Gamma_3^-) \oplus \left(\frac{3N+1}{2}\right)(\Gamma_3^+ \oplus \Gamma_2^-)$	$\left(\frac{3N}{2}\right)(\Gamma_1^+ \oplus \Gamma_3^+ \oplus \Gamma_2^- \oplus \Gamma_3^-)$
Raman	$\frac{(3N-1)}{2}(\Gamma_1^+ \oplus \Gamma_3^- \oplus \Gamma_3^+)$	$\frac{3N}{2}(\Gamma_1^+ \oplus \Gamma_3^+)$
Infrared	$\frac{(3N-1)}{2}(\Gamma_3^+ \oplus \Gamma_2^-)$	$\frac{(3N-2)}{2}(\Gamma_2^- \oplus \Gamma_3^-)$
Acoustic	$\Gamma_3^+ \oplus \Gamma_2^-$	$\Gamma_2^- \oplus \Gamma_3^-$
Silent	$-$	$-$

TABLE IX. Normal vibrational mode irreducible representations (Γ^{vib}) for the N-layer TMDCs at the Γ point within the $1T$-polytype. Raman active, infrared active, acoustic, and silent mode irreducible representations are identified.

	$1T$ polytype	
	N odd	N even
Γ^{vib}	$\left(\frac{3N-1}{2}\right)(\Gamma_1^+ \oplus \Gamma_3^+) \oplus \left(\frac{3N+1}{2}\right)(\Gamma_2^- \oplus \Gamma_3^-)$	$\left(\frac{3N}{2}\right)(\Gamma_1^+ \oplus \Gamma_3^+ \oplus \Gamma_2^- \oplus \Gamma_3^-)$
Raman	$\frac{(3N-1)}{2}(\Gamma_1^+ \oplus \Gamma_3^+)$	$\frac{3N}{2}(\Gamma_1^+ \oplus \Gamma_3^+)$
Infrared	$\frac{(3N-1)}{2}(\Gamma_2^- \oplus \Gamma_3^-)$	$\frac{(3N-2)}{2}(\Gamma_2^- \oplus \Gamma_3^-)$
Acoustic	$\Gamma_2^- \oplus \Gamma_3^-$	$\Gamma_2^- \oplus \Gamma_3^-$
Silent	-	-

group of the wave vector for the Γ point), the Raman tensors are [48]

$$\Gamma_1^+(A_{1g}) : \begin{pmatrix} a & 0 & 0 \\ 0 & a & 0 \\ 0 & 0 & b \end{pmatrix},$$

$$\Gamma_3^+(E_g)_{(1)} : \begin{pmatrix} c & 0 & 0 \\ 0 & -c & d \\ 0 & d & 0 \end{pmatrix}, \quad \Gamma_3^+(E_g)_{(2)} : \begin{pmatrix} 0 & -c & -d \\ -c & 0 & 0 \\ -d & 0 & 0 \end{pmatrix}.$$

For the nonsymmorphic space group for the bulk $2H$ polytype, the Raman tensors are [48]

$$\Gamma_1^+(A_{1g}) : \begin{pmatrix} a & 0 & 0 \\ 0 & a & 0 \\ 0 & 0 & b \end{pmatrix},$$

$$\Gamma_5^+(E_{1g}) : \begin{pmatrix} 0 & 0 & 0 \\ 0 & 0 & c \\ 0 & c & 0 \end{pmatrix}, \quad \begin{pmatrix} 0 & 0 & -c \\ 0 & 0 & 0 \\ -c & 0 & 0 \end{pmatrix},$$

$$\Gamma_6^+(E_{2g}) : \begin{pmatrix} 0 & d & 0 \\ d & 0 & 0 \\ 0 & 0 & 0 \end{pmatrix}, \quad \begin{pmatrix} d & 0 & 0 \\ 0 & -d & 0 \\ 0 & 0 & 0 \end{pmatrix}.$$

III. SUMMARY AND DISCUSSIONS

In this work, symmetry-related aspects of bulk and N-layer $2Ha$, $2Hc$ and $1T$ TMDCs polytypes were discussed from a group theory perspective. The analysis of the presence of inversion symmetry gives different behaviors (in the case of odd number of TLs) for the same number of layers in a given material, with different polytypes. Therefore, it is possible to design experiments to probe, for example, the presence of different polytypes within the same sample, with the same number of layers. The breaking of inversion symmetry is crucial in materials suitable for specific applications, like the development of valleytronic devices, and group theory predictions give directions to researches on how to design their devices to achieve their desired symmetry-related goals.

Some perturbations can lower the symmetry of these thin films and this approach has been used to tune some characteristics of these materials. In a strained MoS_2 monolayer, where the doubly degenerate Raman active mode E' splits into E'^- and E'^+ peaks (depending on the magnitude and symmetry of the strain), an optical band gap was found and its magnitude is approximately linear with strain for both monolayer and bilayer MoS_2 [30,31,49]. By using different TMDCs, it is possible to engineer the optical band gap of interest to the researcher. Another possibility is the piling of different TMDCs to engineer new heterostructures, where

the inversion symmetry is broken with more options made available by using multiple materials. Such heterostructures are expected, for example, to give rise to tunable band gaps from 0.79 to 1.16 eV [9].

The symmetry properties of the vibrational modes were found for the high-symmetry points and lines in the BZ, extending previous knowledge beyond the zone center phonons in TMDCs. One important aspect of this symmetry analysis is that, from symmetry variations, it is possible to predict the difference in phonon modes in these structures. N new Raman-active modes have been observed in few layers TMDCs like in WSe_2 [24]. Density functional theory (DFT) combined with polarization-dependent Raman measurements and group theory were used to understand the first-order Raman spectra. For example, the appearance of the inactive mode B_{2g}^1 in bulk WSe_2 and only for specific laser lines is still not well understood and is usually attributed to resonance effects [24]. However, for N even and N odd few layers, A_{1g} (for N even TLs) and A_1' (for N odd TLs) are both observed at 310 cm^{-1}. Furthermore, the E_{1g} mode at around 175 cm^{-1} in bulk WSe_2 ($2Hc$ polytype) is not measurable under the backscattering configuration along the z direction of light propagation, as well as the E'' mode for 1TL of the same polytype (see the Raman tensors in Sec. II F). In films with $N \geqslant 2$, the E'' mode develops into E_g symmetry, for N-even TLs, and into E' modes for N-odd layers, which are both detectable under $\bar{z}(xx)z$ and $\bar{z}(xy)z$ polarizations (these different behaviors are not related to substrate effects, since these modes are also detected in suspended samples) [24]. The mode at 260 cm^{-1} in bulk WSe_2 was previously attributed to the Raman-active out-of-plane A_{1g} mode, but polarization measurements have shown that even for $\bar{z}(xy)z$ configuration this mode is observed, in contrast with the group theoretical prediction and the previous symmetry assignment. This mode was consequently attributed to second-order Raman scattering [24]. Similar results were observed for $MoTe_2$ [25] and are expected for other TMDCs. The extended group theory analysis described here should be used to guide researchers in making correct mode assignments using the tables and discussion given in the present work.

[1] K. S. Novoselov, A. K. Geim, S. V. Morozov, D. Jiang, Y. Zhang, S. V. Dubonos, I. V. Grigorieva, and A. A. Firsov, Science **306**, 666 (2004).

[2] M. I. Katsnelson, K. S. Novoselov, and A. K. Geim, Nat. Phys. **2**, 620 (2006).

[3] H. Zhang, C. X. Liu, X. L. Qi, X. Dai, Z. Fang, and S. C. Zhang, Nat. Phys. **5**, 438 (2009).

[4] K. K. Kim, A. Hsu, X. Jia, S. M. Kim, Y. Shi, M. Hofmann, D. Nezich, J. F. Rodriguez-Nieva, M. Dresselhaus, T. Palacios, and J. Kong, Nano Lett. **12**, 161 (2011).

[5] A. Splendiani, L. Sun, Y. Zhang, T. Li, J. Kim, C.-Y. Chim, G. Galli, and F. Wang, Nano Lett. **10**, 1271 (2010).

[6] H. R. Gutiérrez, N. Perea-López, A. L. Elías, A. Berkdemir, B. Wang, R. Lv, F. López-Urías, V. Crespi, H. Terrones, and M. Terrones, Nano Lett. **13**, 3447 (2012).

[7] P. Tonndorf, R. Schmidt, P. Böttger, X. Zhang, J. Börner, A. Liebig, M. Albrecht, C. Kloc, O. Gordan, D. R. T. Zahn, S. M. de Vasconcellos, and R. Bratschitsch, Opt. Express **21**, 4908 (2013).

[8] A. K. Geim and I. V. Grigorieva, Nature (London) **499**, 419 (2013).

[9] H. Terrones, F. López-Urías, and M. Terrones, Sci. Rep. **3**, 1549 (2013).

[10] H. Fang, C. Battaglia, C. Carraro, S. Nemsak, B. Ozdol, J. S. Kang, H. A. Bechtel, S. B. Desai, F. Kronast, A. A. Unal, G. Conti, C. Conlon, G. K. Palsson, M. C. Martin, A. M. Minor, C. S. Fadley, E. Yablonovitch, R. Maboudian, and A. Javey, P. Natl. Acad. Sci. USA **111**, 6198 (2014).

[11] M. Chhowalla, H. S. Shin, G. Eda, L. J. Li, K. P. Loh, and H. Zhang, Nat. Chem. **5**, 263 (2013).

[12] Q. H. Wang, K. Kalantar-Zadeh, A. Kis, J. N. Coleman, and M. S. Strano, Nat. Nanotechnol. **7**, 699 (2012).

[13] S. Z. Butler, S. M. Hollen, L. Cao, Y. Cui, J. A. Gupta, H. R. Gutiérrez, T. F. Heinz, S. S. Hong, J. Huang, A. F. Ismach, E. Johnston-Halperin, M. Kuno, V. V. Plashnitsa, R. D. Robinson, R. S. Ruoff, S. Salahuddin, J. Shan, L. Shi, M. G. Spencer, M. Terrones, W. Windl, and J. E. Goldberger, ACS Nano **7**, 2898 (2013).

[14] J. C. Shaw, H. Zhou, Y. Chen, N. O. Weiss, Y. Liu, Y. Huang, and X. Duan, Nano Res. **7**, 1 (2014).

[15] H. Sahin, S. Tongay, S. Horzum, W. Fan, J. Zhou, J. Li, J. Wu, and F. M. Peeters, Phys. Rev. B **87**, 165409 (2013).

[16] L. Britnell, R. M. Ribeiro, A. Eckmann, R. Jalil, B. D. Belle, A. Mishchenko, Y. J. Kim, R. V. Gorbachev, T. Georgiou, S. V. Morozov, A. N. Grigorenko, A. K. Geim, C. Casiraghi, A. H. Castro Neto, and K. S. Novoselov, Science **340**, 1311 (2013).

[17] D. Xiao, G. B. Liu, W. Feng, X. Xu, and W. Yao, Phys. Rev. Lett. **108**, 196802 (2012).

[18] W. Yao, D. Xiao, and Q. Niu, Phys. Rev. B **77**, 235406 (2008).

[19] T. Cao, G. Wang, W. Han, H. Ye, C. Zhu, J. Shi, Q. Niu, P. Tan, E. Wang, B. Liu, and J. Feng, Nat. Commun. **3**, 887 (2012).

[20] K. F. Mak, K. He, J. Shan, and T. F. Heinz, Nat. Nanotech. **7**, 494 (2012).

[21] H. Zeng, G.-B. Liu, J. Dai, Y. Yan, B. Zhu, R. He, L. Xie, S. Xu, X. Chen, W. Yao, and X. Cui, Sci. Rep. **3**, 1608 (2013).

[22] X. Xu, W. Yao, D. Xiao, and T. F. Heinz, Nat. Phys. **10**, 343 (2014).

[23] Y. Zhao, X. Luo, H. Li, J. Zhang, P. T. Araujo, C. K. Gan, J. Wu, H. Zhang, S. Y. Quek, M. S. Dresselhaus, and Q. Xiong, Nano Lett. **13**, 1007 (2013).

[24] X. Luo, Y. Zhao, J. Zhang, M. Toh, C. Kloc, Q. Xiong, and S. Y. Quek, Phys. Rev. B **88**, 195313 (2013).

[25] M. Yamamoto, S. T. Wang, M. Ni, Y.-F. Lin, S.-L. Li, S. Aikawa, W.-B. Jian, K. Ueno, K. Wakabayashi, and K. Tsukagoshi, ACS Nano **8**, 3895 (2014).

[26] L. M. Malard, T. V. Alencar, A. P. M. Barboza, K. F. Mak, and A. M. de Paula, Phys. Rev. B **87**, 201401(R) (2013).

[27] Y. Li, Y. Rao, K. F. Mak, Y. You, S. Wang, C. R. Dean, and T. F. Heinz, Nano Lett. **13**, 3329 (2013).

[28] N. Kumar, S. Najmaei, Q. Cui, F. Ceballos, P. M. Ajayan, J. Lou, and H. Zhao, Phys. Rev. B **87**, 161403(R) (2013).

[29] X. Yin, Z. Ye, D. A. Chenet, Y. Ye, K. O'Brien, J. C. Hone, and X. Zhang, Science **344**, 488 (2014).

[30] H. J. Conley, B. Wang, J. I. Ziegler, R. F. Haglund, Jr., S. T. Pantelides, and K. I. Bolotin, Nano Lett. **13**, 3626 (2013).

[31] Y. Wang, C. Cong, C. Qiu, and T. Yu, Small **9**, 2857 (2013).

[32] J. A. Wilson and A. D. Yoffe, Adv. Phys. **18**, 193 (1969).

[33] H. Katzke, P. Tolédano, and W. Depmeier, Phys. Rev. B. **69**, 134111 (2004).

[34] A. Kormányos, V. Zólyomi, N. D. Drummond, P. Rakyta, G. Burkard, and V. I. Fal'ko, Phys. Rev. B **88**, 045416 (2013).

[35] *International Tables for Crystallography*, 5th ed., Vol. A: Space-Group Symmetry, edited by T. Hahn (Springer, Dordrecht, The Netherlands, 2005).

[36] L. Hromadová, R. Martoňák, and E. Tosatti, Phys. Rev. B **87**, 144105 (2013).

[37] *International Tables for Crystallography*, 1st ed., Vol. E: Subperiodic groups, edited by T. Kopský and D. B. Litvin (Kluwer, Dordrecht, The Netherlands, 2002).

[38] L. M. Malard, M. H. D. Guimarães, D. L. Mafra, M. S. C. Mazzoni, and A. Jorio, Phys. Rev. B **79**, 125426 (2009).

[39] M. Tinkham, *Group Theory and Quantum Mechanics* (Dover, Mineola, New York, 2012).

[40] M. S. Dresselhaus, G. Dresselhaus, and A. Jorio, *Group Theory: Application to the Physics of Condensed Matter* (Springer-Verlag Berlin, Germany, 2008).

[41] P. W. M. Jacobs, *Group Theory with Applications in Chemical Physics* (Cambridge University Press, New York, 2005).

[42] W. T. Hsu, Z. A. Zhao, L. J. Li, C. H. Chen, M. H. Chiu, P. S. Chang, Y. C. Chou, and W. H. Chang, ACS Nano **8**, 2951 (2014).

[43] R. W. Boyd, *Nonlinear Optics* (Academic, Burlington, MA, USA, 2008).

[44] Y. R. Shen, *The Principles of Nonlinear Optics* (John Wiley & Sons, Hoboken, NJ, 2003).

[45] See Supplemental Material at http://link.aps.org/supplemental/10.1103/PhysRevB.90.115438 for character tables (with the notation conversion from space group to point group, for all the GWV used in this work) and for tables for the irreducible representations for lattice vibrations (Γ^{vib}) for bulk 2*H* and 1*T* polytypes.

[46] Bilbao Crystallographic Server, http://www.cryst.ehu.es/cgi-bin/cryst/programs/nph-doc-raman.

[47] T. C. Damen, S. P. S. Porto, and B. Tell, Phys. Rev. **142**, 570 (1966).

[48] R. Loudon, Adv. Phys. **13**, 423 (1964).

[49] A. Castellanos-Gomez, R. Roldán, E. Cappelluti, M. Buscema, F. Guinea, H. S. J. van der Zant, and G. A. Steele, Nano Lett. **13**, 5361 (2013).